RESEARCH ARTICLE

Journal of Cellular Physiology **WILEY**

3D printed controllable microporous scaffolds support embryonic development in vitro

Jia Guo[1,2,3] | Yuanyuan Li[1,2,3,4] | Zili Gao[1,2,3] | Jiawei Lyu[2,3,5] | Wenli Liu[1,2,3] | Yongchao Duan[2,3,5] | Lixun Zhou[1,2,3] | Qi Gu[1,2,3] (iD)

[1]The State Key Laboratory of Membrane Biology, Institute of Zoology, Chinese Academy of Sciences, Beijing, China

[2]Beijing Institute for Stem Cell and Regenerative Medicine, Beijing, China

[3]University of Chinese Academy of Sciences, Beijing, China

[4]Department of Nephrology, Postdoctoral Workstation, Precision Medicine Center of Shanxi Provincial People's Hospital, The Affiliated People's Hospital of Shanxi Medical University, Shanxi Kidney Disease Institute, Taiyuan, China

[5]The State Key Laboratory of Stem Cell and Reproductive Biology, Institute of Zoology, Chinese Academy of Sciences, Beijing, China

Correspondence
Qi Gu, The State Key Laboratory of Membrane Biology, Institute of Zoology, Chinese Academy of Sciences, Beijing 100101, China.
Email: qgu@ioz.ac.cn

Abstract

Little is known about the complex molecular and cellular events occurring during implantation, which represents a critical step for pregnancy. The conventional 2D culture could not support postimplantation embryos' normal development, and 3D conditions shed light into the "black box". 3D printing technology has been widely used in recapitulating the structure and function of native tissues in vitro. Here, we 3D printed anisotropic microporous scaffolds to culture embryos by manipulating the advancing angle between printed layers, which affected embryo development. The 30° and 60° scaffolds promote embryo development with moderate embryo-scaffold attachments. T-positive cells and FOXA2-positive cells were observed to appear in the posterior region of the embryo and migrated to the anterior region of the embryo on day 7. These findings demonstrate a 3D printed stand that supports embryonic development in vitro and the critical role of 3D architecture for embryo implantation, in which additive manufacturing is a versatile tool.

KEYWORDS
3D printing, anisotropic microporous scaffolds, embryo implantation, in vitro culture

1 | INTRODUCTION

Elucidating the characteristics of embryonic development is an important research topic in developmental biology. Embryo development provides an essential theoretical basis for reproductive health and supports the development of tissue-engineered reconstructed organs. Due to the limited characteristic strategies of embryo development in vivo, current research mainly focuses on the preimplantation stage of mammalian embryogenesis (Wang et al., 2018; Zheng & Xie, 2019). Studies on postimplantation development are limited due to the inability to observe

---

Jia Guo and Yuanyuan Li contributed equally to work.

them directly (Aguilera-Castrejon et al., 2021; Fu et al., 2021). Therefore, postimplantation research on embryos is critical for understanding the development of embryos, tissues, and organs (Bedzhov & Leung, Bialecka, et al., 2014). At present, the main methods of postimplantation embryo culture are 2D based tissue culture plates (Wu et al., 1981). In recent years, with the development and application of novel biomaterials (He, 2017; Huang et al., 2017), biomaterials are also used for in vitro culture of postimplantation embryos, such as (1) tissue culture plates coated with collagen, laminin, or fibronectin (Carson et al., 1988; Hsu, 1973). (2) coculture with uterine endothelial cells (Salomon & Sand Sherman, 1975). (3) polyacrylamide hydrogel coated plate (Kauma & Wand Matt, 1995). (4) matrigel basement membrane matrix (Harrison et al., 2017; Shahbazi et al., 2017). Biomaterials were used to culture mouse blastocysts to the E6.75 stage (Bedzhov & Leung, Bialecka, et al., 2014). However, culture techniques still have many problems, such as the complexity of the culture plate, insufficient gas exchange (Bedzhov & Leung, Bialecka, et al., 2014), and the physical properties of the culture plate different from the natural uterus (Filas et al., 2011; Manoogian et al., 2008). The potential reason for this is that these techniques mainly rely on 2D culture systems (Gu et al., 2020). Govindasamy et al. (2021) have used hydrogels to explore the impact of 3D environment on embryo implantation.

3D printing technology can form highly reproducible and precisely controlled structures (Cui et al., 2017), and it can be used to simulate the complex structure of biological tissues (Hull et al., 2022). 3D printing has been increasingly applied in tissue engineering (Do et al., 2015; Raja & Yun, 2016). Complicated architectures of various tissues such as the liver (Liu et al., 2021; Yang et al., 2021), heart (Ma et al., 2014), blood vessels (Peng et al., 2021; Zhou et al., 2020), and tumors have been fabricated (Huang et al., 2014). 3D printing holds the advantage of building spatial structures mimicking the living environment of cells in vivo (Hossain et al., 2021). The uterus is the carrier of embryonic development in the body, and the patients whose uterus cannot conceive account for 38% of infertility symptoms (Zegers-Hochschild et al., 2009). The artificial uterus may bring hope to infertile patients (Campo et al., 2017), and 3D printing can promote embryonic development, a possible solution could be found in the field of uterine regeneration.

In addition, 3D printing could modulate porosity and nutrient penetration through anisotropic microporous design (Engelmayr et al., 2008; Yoo, 2013; Zhu et al., 2019), provide mechanical support for cells (Engelmayr et al., 2008; Harrison et al., 2017), and be used to study cell-scaffold interactions (Hollister, 2006). Laronda proposed that 3D-printed microporous hydrogel scaffolds can effectively promote the maturation of oocytes (Laronda et al., 2017). Still, there are few reports on the application of 3D printing technology in embryo development. 3D culture of postimplantation embryos requires porous channels for nutrient penetration, migration, and attachment (Hollister, 2006) and 3D printing offers hope for building a uterus in vitro.

Here, we used 3D printing technology to construct anisotropic microporous scaffolds with different angles using polydimethylsiloxane (PDMS), a biomaterial used for culturing embryos (Ozbolat et al., 2018; Weimar et al., 2013). We characterized the properties of the stands at different angles, their ability to support embryos in vitro, the interaction between embryos and substrates, and the developmental states of embryos on 3D printed anisotropic microporous scaffolds. With the scaffolds improving embryo development in vitro, 3D printing will allow new research opportunities into reproductive biology and regenerative medicine.

2 | MATERIALS AND METHODS

2.1 | Animals

All animals were purchased from SPF Biotechnology. All experimental procedures involving animals were approved and implemented following the animal use guidelines outlined by the Animal Care and Use Committee of the Institute of Zoology, Chinese Academy of Sciences (Ethical approval No. IOZ20180058).

2.2 | Materials

The reagents used in this study were as follows: PDMS (SE1700; DOWSIL), CMRL 1066 (11530037; Invitrogen), penicillin-streptomycin (60162ES76; YEASEN), fetal bovine serum (FBS) (SE200-ES; Vistech), GlutaMAX™ Supplement (35050061; Thermo), Sodium Pyruvate (11360070; Thermo), MEM Non-Essential Amino Acids Solution (11140050; Thermo), N-2 Supplement (17502048; Gibco), B-27™ Supplement (17504044; Gibco), KnockOut™ Serum Replacement (10828028; Gibco), glucose (D9434; Sigma), 4% fixative solution (P1110; Solarbio), Triton-100 (9002-93-1, Sigma), Tween-20 (P1379-25; Sigma), FOXA2 (8186S; Cell Signaling Technology), OCT4 (sc-5279; Santa Cruz), SOX2 (ab97959; Abcam), EOMES (ab23345; Abcam), T (ab209665; Abcam), and Phall (40737ES75; Yeasen). Alexa 488 goat anti-rabbit (A11034; Invitrogen), Cyanine3 goat anti-rabbit (A10520; Invitrogen), Hoechst 33342 (H3570; Invitrogen).

2.3 | Bioprinting process

The anisotropic microporous scaffolds were designed using SolidWorks software 2018. The mass ratio of the matrix and crosslinker in the PDMS prepolymer was set to 10:1, loaded into the printing cylinder and centrifuged at 4000g for 3 min to remove air bubbles. Scaffolds were printed using a pneumatic extrusion-based 3D printing system (Bio-Architect®-WS) and a customized 3D bioprinter (SIA bioprinter PRO) developed by the Shenyang Institute of Automation, Chinese Academy of Sciences (Wang et al., 2021). Stands were printed with a needle (200 μm) at an air pressure of 0.3 MPa and the speed was 8 mm/s. The PDMS scaffolds were cured at 80°C for 2 h and autoclaved before use.

2.4 | Scanning electron microscopy

At 4°C, the PDMS scaffolds or embryos were fixed for 4 h in 2.5% glutaraldehyde. The samples were then dehydrated for 10 min in 30%, 40%, 50%, 60%, 70%, 80%, and 90% ethanol and for 30 min in 100% ethanol. After supercritical drying (CPD300; Leica), the samples were coated with platinum (ACE600; Leica) for scanning electron microscopy (SU8010; Hitachi).

2.5 | Embryo acquisition and culture

Pregnant mice were humanely euthanized 3.5 days postcoitum through cervical dislocation. The embryos were flushed out with a flush medium and seeded onto the PDMS scaffolds, then incubated at 37°C in 5% CO_2.

(1) Flush medium: CMRL 1066 + 5 × penicillin-streptomycin + 10% FBS.
(2) Medium for embryos on IVC days 0–1: CMRL 1066 + 1 × penicillin-streptomycin + 1 × GlutaMAX™ supplement + 1 × MEM nonessential amino acids solution + 1 × sodium pyruvate + 0.5 × N-2 supplement + 0.5 × B-27™ supplement + 10% FBS + 0.5 mg/ml matrigel.
(3) Medium for embryos on IVC day 2: CMRL 1066 + 1 × penicillin-streptomycin + 1 × GlutaMAX™ supplement + 1 × MEM nonessential amino acids solution + 1 × sodium pyruvate + 0.5 × N-2 supplement + 0.5 × B-27™ supplement + 20% FBS.
(4) Medium for embryos on IVC days 3–4: CMRL 1066 + 1 × sodium pyruvate 1 × penicillin-streptomycin + 1 × GlutaMAX™ supplement + 1 × MEM nonessential amino acids solution + 30% Knock-Out™ serum replacement.
(5) Medium IV for embryos on IVC days 5–6: CMRL 1066 + 1 × penicillin-streptomycin + 1 × GlutaMAX™ supplement + 1 × MEM nonessential amino acids solution + 1 × sodium pyruvate + 30% KnockOut™ serum replacement + 30% RS (rat serum) + 0.5 mg/ml glucose.

2.6 | Identification of embryos on PDMS scaffolds

The embryos were fixed for 6 h with 4% PFA at 4°C, permeabilized for 6 h in 1% Triton X-100 in phosphate-buffered saline (PBS) at 4°C, blocked for 6 h in 0.1% Tween-20, 0.01% Triton X-100 and 1% bovine serum albumin in PBS at 4°C, and incubated with primary antibodies at 4°C overnight. The primary antibodies used were FOXA2 (1:100), OCT4 (1:100), SOX2 (1:100), EOMES (1:100), T (1:100), and Phalloidin (1:500). The following secondary antibodies and nuclear staining were incubated for 6 h at 4°C: Alexa 488 goat anti-rabbit (1:500), Cyanine3 goat anti-rabbit (1:500) and Hoechst 33342 (1:1000). Embryos were imaged using a Zeiss LSM 880 confocal microscope.

2.7 | Contact angle measurements

Contact angle measurements were conducted using KRÜSS's contact angle machine KRÜSS ADVANCE software version 1.11.0.15801. Before testing, for the sessile drop technique, a water droplet of 2 µl was deposited on a PDMS, in which plasma was treated for different durations and measured within 5 s. Then, the analysis of contact angles from the recorded videos was performed using ImageJ software.

2.8 | Rheological measurement

Rheological measurements were performed using an MCR 302 rheometer (Anton Paar) with a 25 mm diameter parallel plate geometry measuring system. The storage modulus (G′) and loss modulus (G″) were recorded from the amplitude sweep of Inks 10:1 at a constant frequency of 1 Hz at a strain range from 0.01% to 100%. A frequency sweep was carried out to obtain G′, G″ at a continuous strain of 1%, which was within the linear viscoelastic range at a frequency range from 100 to 0.1 Hz. The flow and viscosity curves were obtained from the rotational test, which was carried out at shear rates ranging from 0.01 to 100 s^{-1}

2.9 | Statistical analysis

The embryos were randomly allocated to each group. GraphPad Prism v.7.0 and ImageJ software were used for all statistical analyses of the results obtained. Data were checked for normal distribution and equal variances before each parametric statistical test were performed. One-way analysis of variance tests was performed with Welch's correction if the variance between groups was not equal. All quantitative data were presented as the mean ± standard deviation. All experiments were repeated at least three times (the repeat number is indicated as n in the figure legends).

3 | RESULTS

3.1 | Fabrication of PDMS anisotropic microporous scaffolds with different angles using 3D printing

Mouse embryos develop in the uterus after implantation (Weimar et al., 2013). Therefore, we used 3D printing combined with biomaterials to provide embryos with a culture environment in terms of contact angles and embryo-scaffold interactions (Figure 1a). Regarding the printed scaffolds, the angle of the rods, spacing, and other conditions impact the porosity, wettability, and attachment area. Based on this, the 3D printing strategy for constructing a culture anisotropic microporous scaffold in this study was as follows: Step 1, with an advancing angle of 0°, a thickness of 200 µm; Step 2, the middle layer was printed with different advanced angles (0°, 30°, 60°, and 90°), 200 µm thickness; and Step 3, based on the
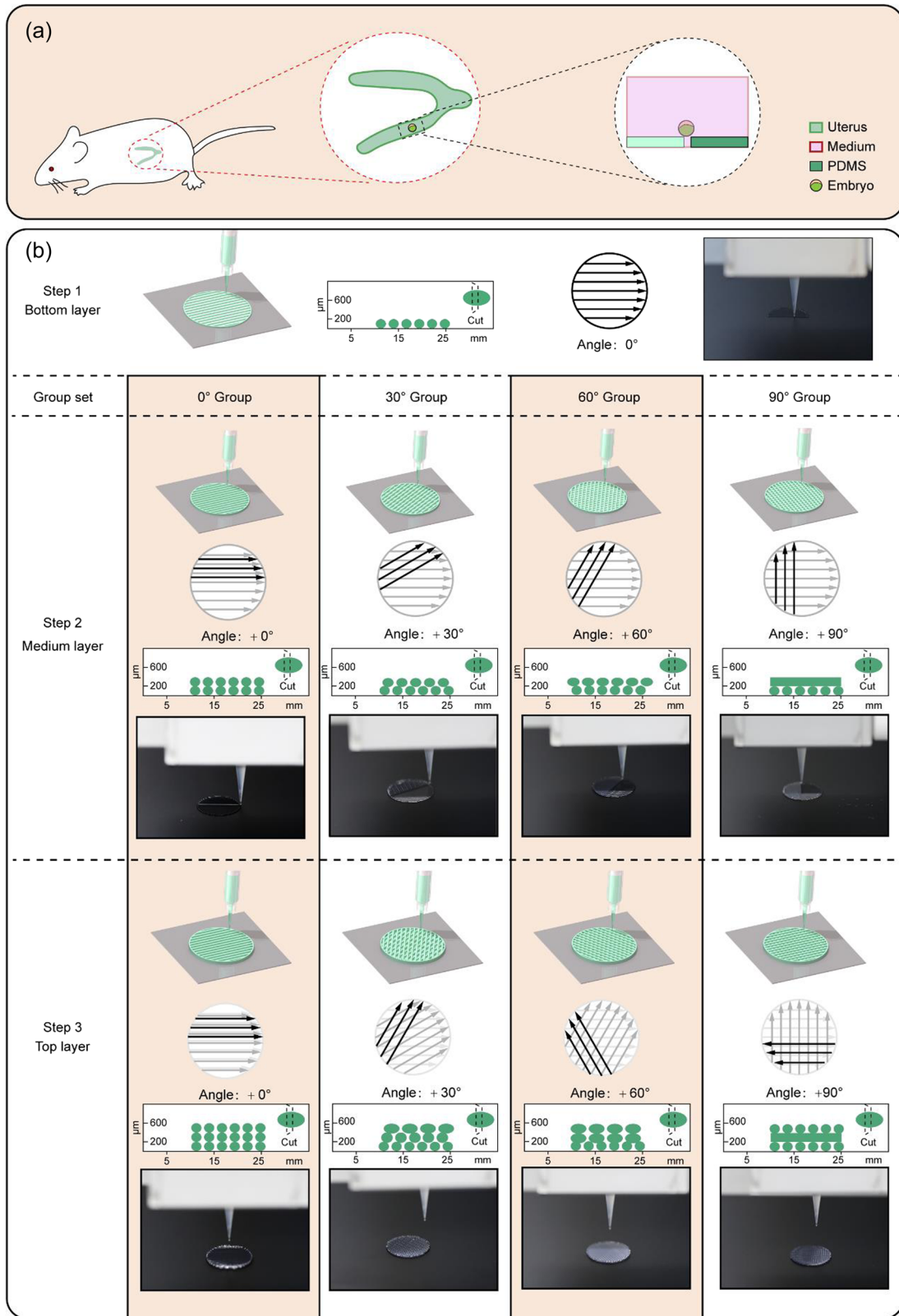
FIGURE 1 Simplified illustrations of 3D bioprinting strategies used in this study. (a) Schematic of the embryo implantation in vivo (left panel). Schematic of the embryo culture in vitro (right panel). (b) Automated device printing on a 15 mm glass slide substrate in three sequential steps. The first step is to print the basic steps of all angles, the printed angle defined as 0°; a corresponding image from the printing procedure is displayed. In print step 1, a 200-μm layer was printed. In printing step 2, the 200-μm layer was printed at 0°, 30°, 60° and 90°. In printing step 3, the 200-μm layer was sequentially printed at 0°, 60°, 120°, 180°.

middle layer, again with different advance angles, 200 μm thickness (Figure 1b). The printed anisotropic microporous scaffolds were cured at 80°C for 2 h, and after aseptic processing, scaffolds with different parameters such as porosity, wettability, and contact area were obtained for subsequent embryo culture.

PDMS was chosento achieve the above printing strategy because of its superior printing performance (Bhattacharjee et al., 2018; Ferraz et al., 2020; Ozbolat et al., 2018) and its biocompatible properties (Harrison et al., 2017; Hiramatsu et al., 2013). The printing performance of PDMS with matrix and crosslinker = 10:1 (the ratio
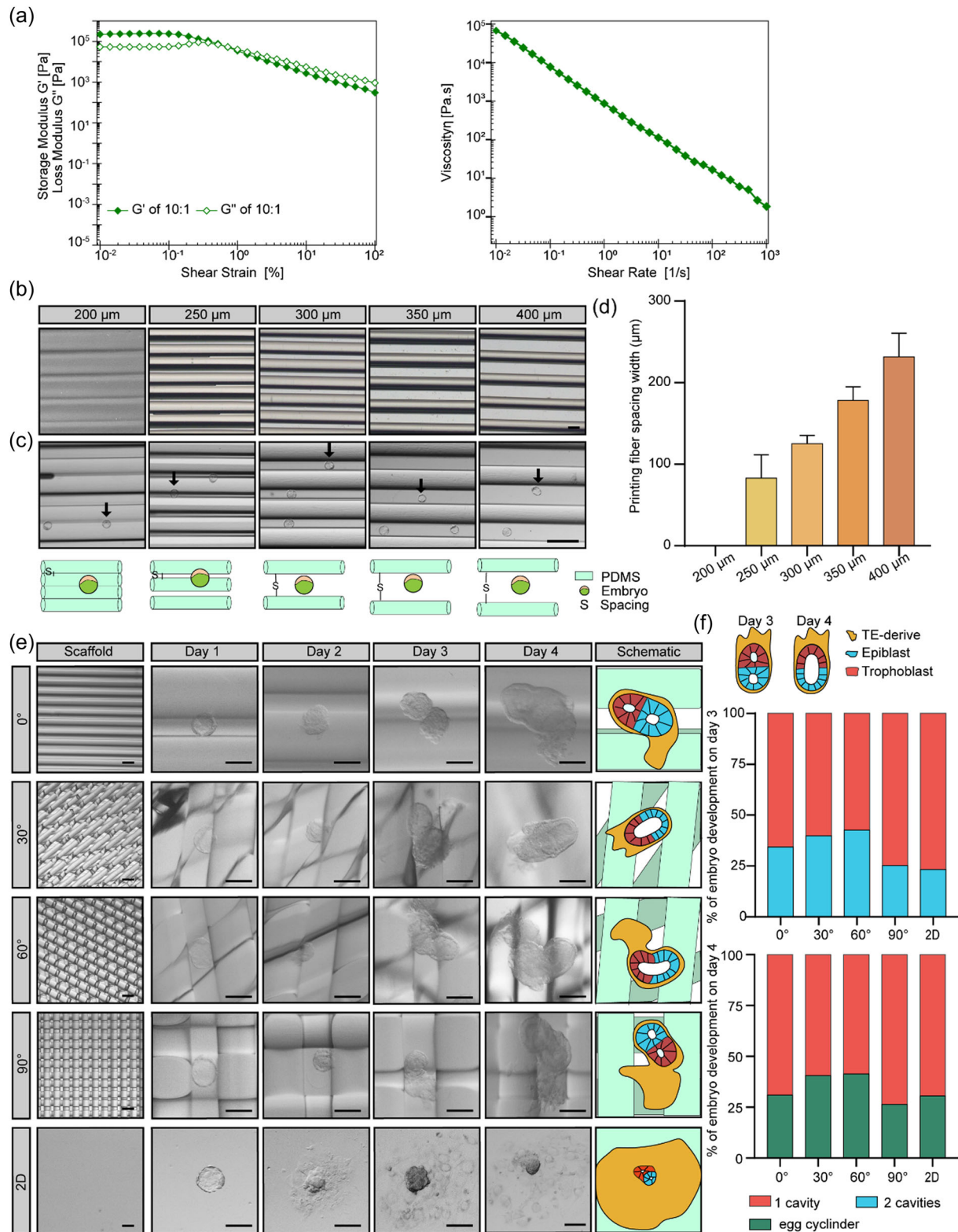

FIGURE 2 (See caption on next page)

applied in embryo culture was examined). G′ > G″ showed that PDMS has typical elastic properties; when the strain reached a certain level, G′ < G″, it turned into a liquid (left panel, Figure 2a), demonstrating shear-thinning properties (right panel, Figure 2a). The 200-μm needle was selected for printing because of the need for stable and long-term printing. The print spacing may impact embryo development, and E3.5 embryos are approximately 100 μm in size. First, PDMS microporous scaffolds of 200-, 250-, 300-, 350-, and 400-μm print spacings were used. The print spacings of 200- and 250-μm print spacings were discarded because there was no gap tocause the printed fibers to stick each other (Figure 2b). The 300-, 350-, and 400-μm print spacing had uniform gaps, but the 350- and 400-μm print spacings were discarded because the obtained gap was larger than the diameter of the embryo, which was not conducive for embryo culture (Figure 2c,d). Therefore, we found the 300-μm printed spacing to be the most suitable for the experiment. In summary, a 10:1 PDMS printing material, 200-μm printing needle, and 300-μm print spacing were determined to be optimal for printing.

3.2 | Embryo development on 3D printed scaffolds

According to this printing strategy, anisotropic microporous scaffolds were constructed at different advancing angles (0°, 30°, 60°, and 90°) to obtain platforms with uniform morphologies (left panel, Figure 2e). E3.5 embryos were seeded on anisotropic microporous scaffolds with different angles and a culture system of 2D PDMS to study the effect of anisotropic microporous scaffolds on embryo development. On day 1 of in vitro culture, embryos were attached between or on the printed fibers of the 0° and 90° anisotropic microporous scaffolds and the lower or slant fibers of the 30° and 60° anisotropic microporous scaffolds (Figure 2e). On day 3 of in vitro culture, the efficiencies of embryos forming 2 cavities (EPI cavity and EXE cavity) were 34.26 ± 7.60%, 39.76 ± 12.71%, 42.61 ± 8.62%, 25.18 ± 6.55% and 23.17 ± 7.8%. On day 4 of in vitro culture, the efficiencies of embryo forming the egg cylinder were 30.79 ± 10.09%, 40.52 ± 12.68%, 41.36 ± 8.33%, 26.37 ± 8.29% and 30.61 ± 14.91%, respectively (Figure 2e,f). Overall, the mechanical support provided by the 30° and 60° anisotropic microporous scaffolds best facilitated embryonic development.

3.3 | Embryo locations on microporous scaffolds

We speculated that different contact patterns for the embryos were determined by different anisotropic microporous scaffolds, in which the 30° and 60° ones more favorable for the in vitro culture of embryos. Differences in scaffolds are detected, including the porosity and wettability (contact angle). SEM results indicated that the porosity of the 30° and 60° anisotropic microporous scaffolds were similar (Figure 3a). The 0° anisotropic microporous scaffolds had a larger porosity, while the 90° anisotropic microporous scaffolds and 2D PDMS had a small porosity (Figure 3b). The contact angles of the anisotropic microporous scaffolds were measured (Figure 3c) approximately 130° for the anisotropic microporous scaffolds untreated with plasma. There was no difference between the different anisotropic microporous scaffolds. After plasma treatment for 3 min, the contact angles of the 30° and 60° anisotropic microporous scaffolds were maintained at approximately 55°, and the contact angles of 0° and 90° anisotropic microporous scaffolds and 2D PDMS were all 0° (Figure 3d).

Interestingly, embryo spreading areas after attachment varied by the angle of anisotropic microporous scaffolds. Therefore, the contact area of the embryos at different angles of the anisotropic microporous scaffolds was further examined. Embryos on day 2 of in vitro culture were stained for the cytoskeleton, and the embryo attachment area was smaller on the 30° and 60° anisotropic microporous scaffolds compared to the 0° and 90° anisotropic microporous scaffolds and 2D PDMS (Figure 3e,f, Movies S1–S5). The above results indicated that the 90° anisotropic microporous scaffolds and 2D PDMS had minimal porosity, large attachment area and wettability. The 0° anisotropic microporous scaffolds had a larger porosity, wettability and attachment area. The 30°and the 60° anisotropic microporous scaffolds had suitable porosity, wettability, and attachment area. In conclusion, the 30° and 60° anisotropic microporous scaffolds had the smallest attachment area.

3.4 | OCT4 positive cells in embryos affected by microporous scaffolds

Trophoblast (TE)-derived cells were directly exposed to the uterus after embryo implantation (Aplin & Dand Ruane, 2017; Ozbolat et al., 2018). Therefore, we assumed that the TE-derived cells were in

FIGURE 2 In vitro culture blastocyst on 3D printed anisotropic microporous scaffolds. (a) Measurements of the storage modulus (G′) and loss modulus (G″) were recorded from an amplitude sweep of Inks 10:1 at a constant frequency of 1 Hz at a strain range from 0.01% to 100% (left panel). The viscosity of PDMS 10:1 from rotational testing from $0.01\,s^{-1}$ to $1000\,s^{-1}$ (right panel) was measured. (b) Representative bright-field images of different spacings of PDMS scaffolds. Scale bar = 200 μm. (c) The spacings of PDMS scaffolds were counted. The actual value of spacing of fibers of 200 μm is 0 μm, 250 μm is 82.88 ± 28.76 μm, 300 μm is 125.1 ± 9.91 μm, 350 μm is 178.3 ± 16.65 μm, 400 μm is 231.7 ± 29.04 μm, n = 4 PDMS scaffolds. (d) Representative bright-field images (top panel) and schematic (bottom panel) of embryos on different spacings of PDMS scaffolds. Arrows indicate embryo location. Scale bar = 200 μm. (e) Representative bright-field images and schematic of different angles of PDMS scaffolds and 2D PDMS. Representative bright-field images of embryos were cultured on different angles of PDMS scaffolds and 2D PDMS from days 1 to 4. Scale bars = 100 μm. Day, in vitro culture day. (f) The percentages of embryos on a different angle of PDMS scaffolds with 2 cavities on in vitro culture day 3, egg cylinder on in vitro culture day 4, n = 90 (0°), 119 (30°), 79 (60°), 93 (90°), 81 (2D PDMS) embryos from four independent experiments. Two cavities (EPI cavity [blue area] and ExE cavity [red area]) on in vitro culture day 3, egg cylinder on in vitro culture day 4 (blue area and red area merged). PDMS, polydimethylsiloxane.
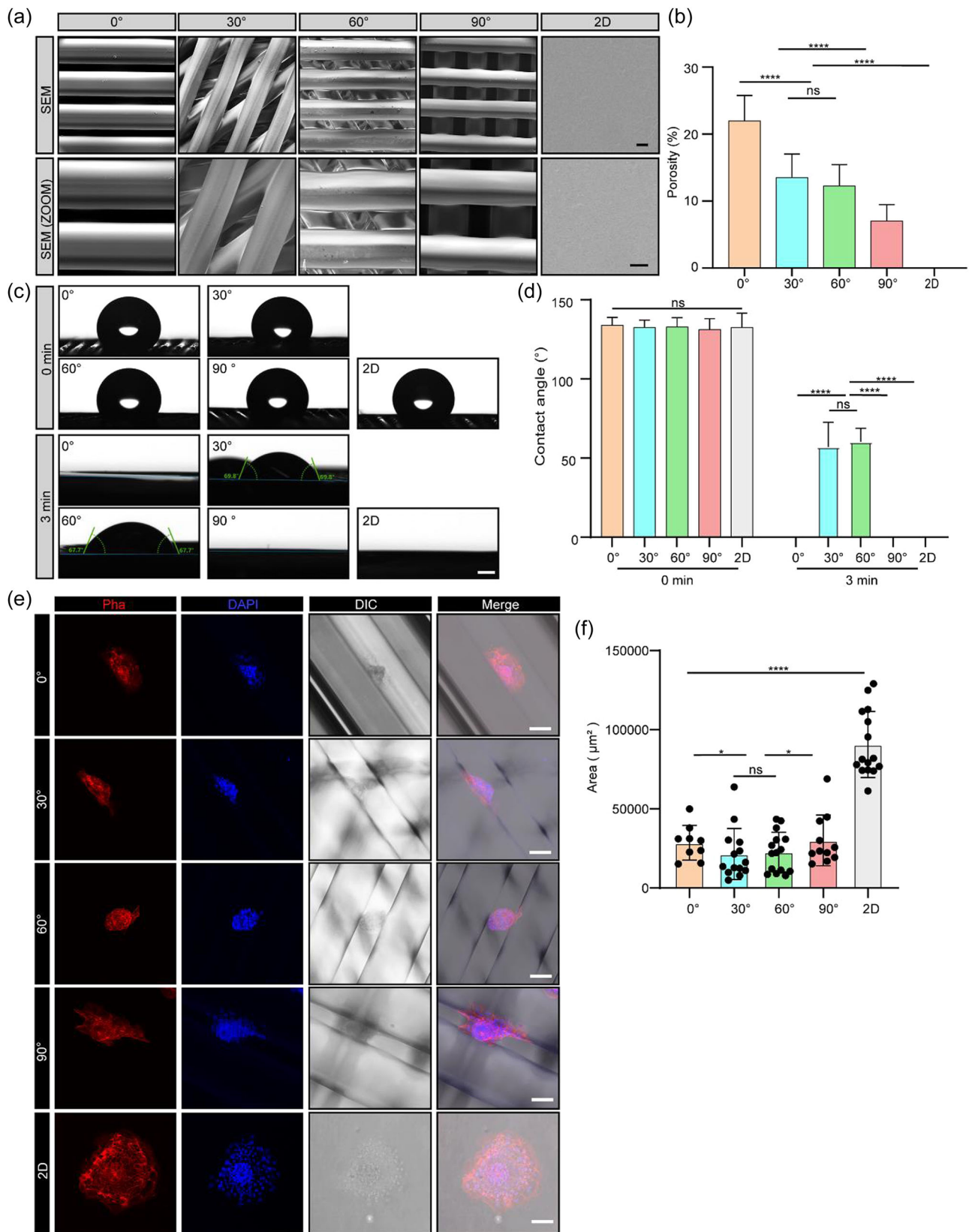
FIGURE 3 (See caption on next page)

direct contact with PDMS on the anisotropic microporous scaffold culture system. We examined the gene expression of significant developmental markers on day 2 of the in vitro culture to test this hypothesis. EOMES is the primary marker of TE-derived cells, which develops into extraembryonic tissue in the future (Harrison et al., 2017). Cells directly in contact with PDMS were EOMES-positive- TE-derived cells (Figure 4a). OCT4-positive cells are epiblast cells that develop into the embryoid body part in the future (Bedzhov & Zernicka-

Goetz, 2014; Plachta et al., 2011). The 30° and 60°anisotropic microporous scaffolds had a higher proportion of OCT4-positive cells, while the 0° and 90° anisotropic microporous scaffolds and 2D PDMS had a lower proportion of OCT4-positive cells (Figure 4b). Furthermore, the ratio of OCT4-positive cells was negatively correlated with the attachment area. In conclusion, 30° and 60° anisotropic microporous scaffolds were more conducive to supporting embryonic development.
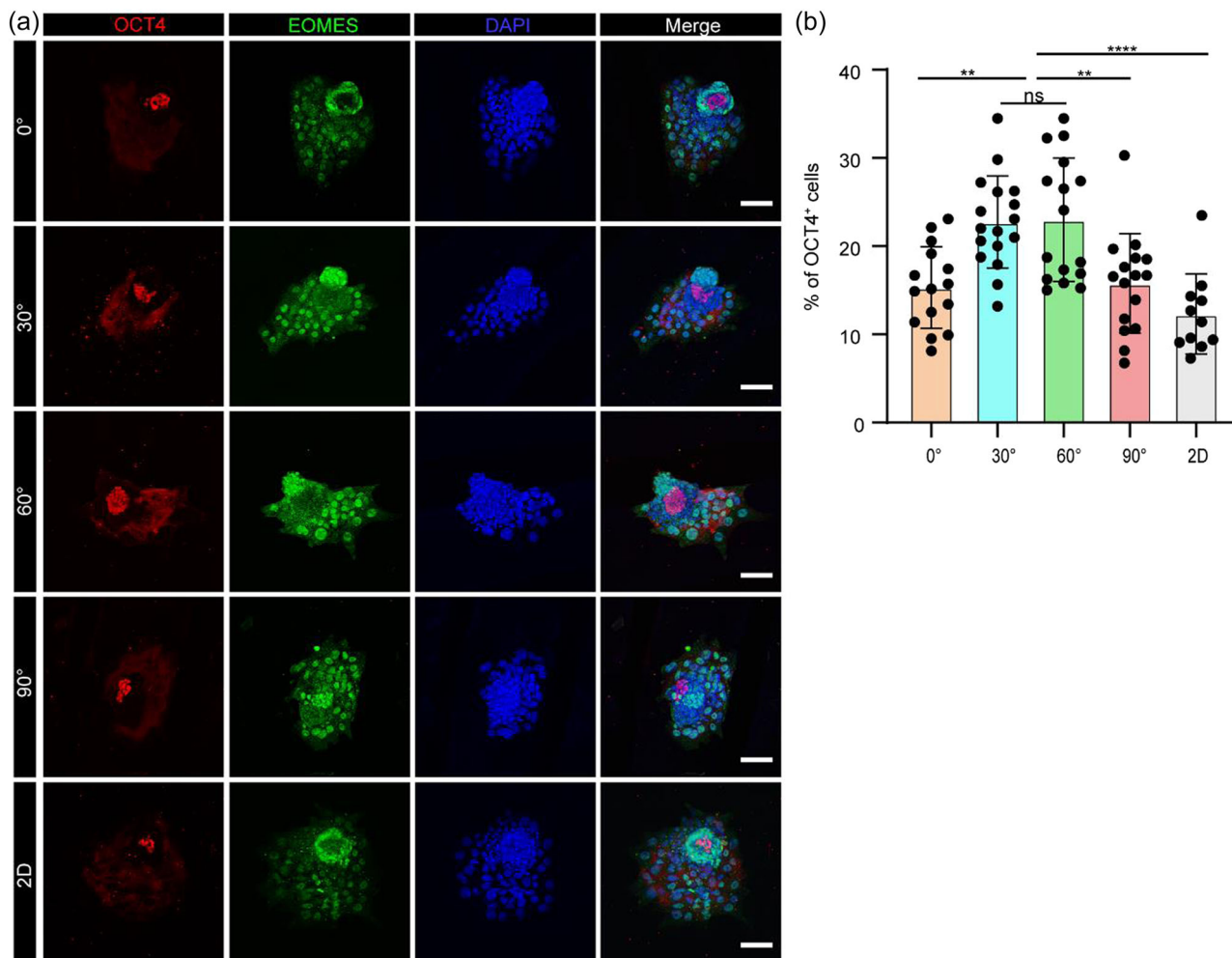

FIGURE 4 The proportion of OCT4+ cells is dependent on the scaffold. (a) In vitro culture day 2 embryos cultured on the different angles of PDMS scaffolds and 2D PDMS labeled by antibodies against Oct4 (red, labeling epiblast) and against EOMES (green, labeling trophoblast), and DAPI (blue, labeling nuclei). Scale bars = 100 μm. (b) Proportion of the OCT4-positive cells. n = 15 (0°), 17 (30°), 16 (60°), 16 (90°), 11 (2D PDMS) embryos. One-way ANOVA test. ns, no significance, $**p < 0.01$, $****p < 0.0001$. ANOVA, analysis of variance; PDMS, polydimethylsiloxane.

FIGURE 3 Embryos interact with scaffolds. (a) SEM images of the different angles of PDMS scaffolds and 2D PDMS (top panel), zoom SEM image (bottom panel). Scale bars = 100 μm. One-way ANOVA test, ns, no significance, $****p < 0.0001$. (b) The statistics of the porosity for SEM images of the different angles of PDMS scaffolds and 2D PDMS. (c) Bright-field images of contact angle measurements with different PDMS scaffolds and 2D PDMS angles for 0 and 3 min of plasma treatment 30 w. Scale bars = 500 μm. (d) The statistics of contact angles with different angles of PDMS scaffolds and 2D PDMS for 0 and 3min of plasma treatment. One-way ANOVA test, no significance; ns, $****p < 0.0001$. n = 3 independent experiments. (e) Immunostaining of Phalloidin (red) for embryos at different angles of PDMS scaffolds and 2D PDMS. Scale bars = 100 μm. (f) The statistics of the embryonic spreading area of the different angles of PDMS scaffolds and 2D PDMS. n = 10 (0°), 14 (30°), 16 (60°), 12 (90°), 15 (2D PDMS) embryos. One-way ANOVA test, ns, no significance, $*p < 0.05$, $****p < 0.0001$. ANOVA, analysis of variance; PDMS, polydimethylsiloxane.
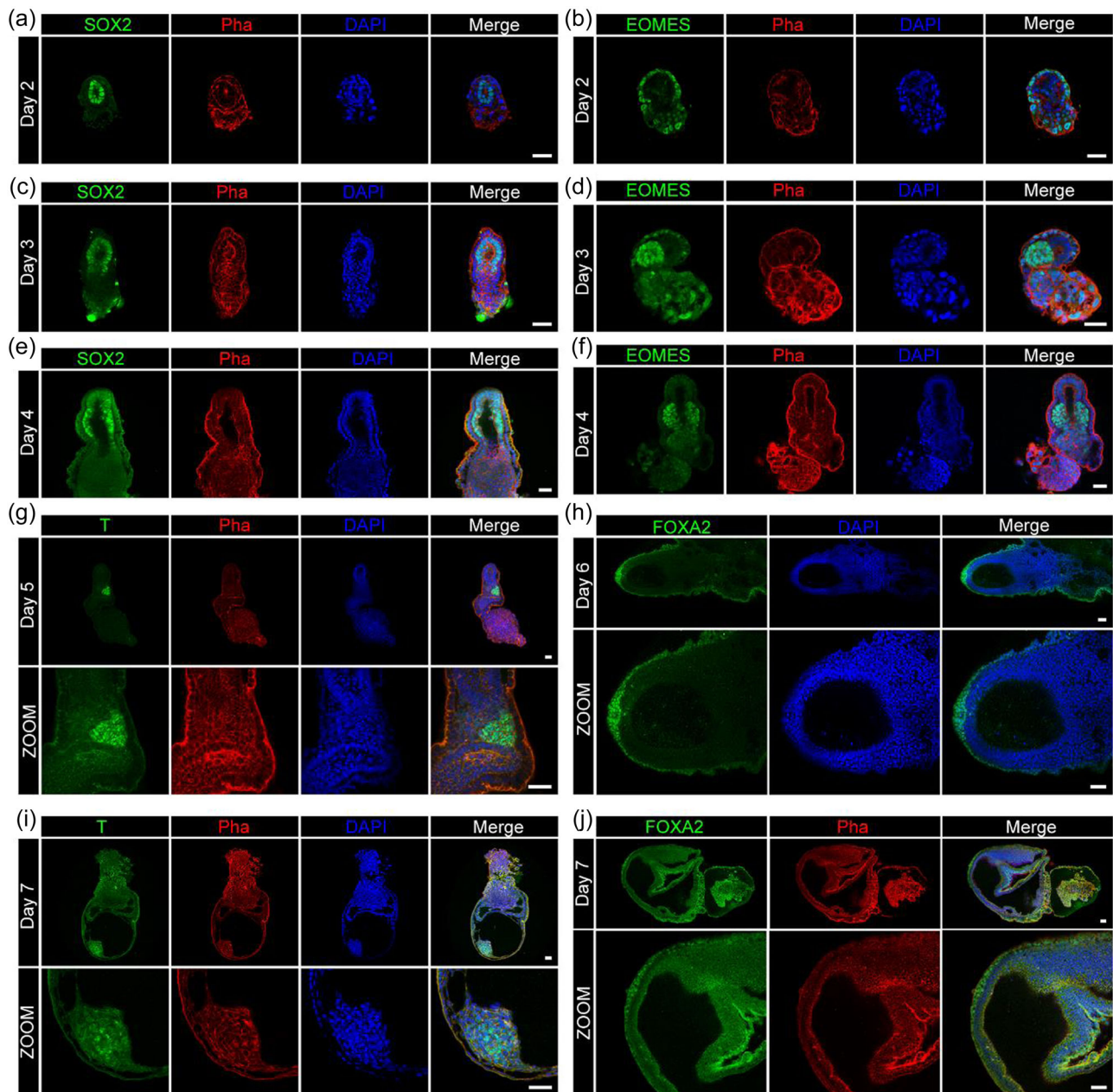
FIGURE 5 Characterization of embryos from days 2 to 7 in vitro. (a–f) In vitro culture days 2–4 embryos on 30° of PDMS scaffolds labeled by antibodies against Sox2 (green, labeling epiblast), against EOMES (green, labeling trophoblast), and Phalloidin (red, labeling cytoskeleton). $n = 3$ independent experiments. Scale bars = 100 μm. (g, i) In vitro culture day 5 or 7 embryos on 30° of PDMS scaffolds stained by an antibody against T (green, labeling primitive streak cells), and Phalloidin (red). Magnified region (bottom panel). $n = 3$ independent experiments. Scale bars = 100 μm. (h, j) In vitro culture day 6 or 7 embryos on 30° PDMS scaffolds stained by an antibody against FOXA2 (green, labeling DVE marker) and Phalloidin (red). Magnified region (bottom panel). $n = 3$ independent experiments. Scale bars = 100 μm. PDMS, polydimethylsiloxane.

3.5 | Embryonic gastrulation supported by 3D-printed microporous scaffolds

Since the 30° and 60° anisotropic microporous scaffolds were more conducive to supporting embryos' development, it needs to define whether the anisotropic microporous scaffolds could further support embryo culture in vitro. Embryos began to undergo apoptosis after 7 days of in vitro culture. Embryos were identified at various stages.

Embryos contacted anisotropic microporous scaffolds on day 1 of in vitro culture followed by being attached to anisotropic microporous scaffolds on day 2 of in vitro culture. SOX2 (EPI) positive cells formed in the center of the embryo and formed a rosette-like configuration, and the SOX2 (EPI) positive cells were surrounded by EOMES-positive TE cells (Figure 5a,b), at this stage, the embryos were similar to E4.5 embryos in vivo (S1a,b). On day 3 of in vitro culture, the EPI cavity of SOX2-positive cells expanded, and EOMES-positive cells

formed ExE cavities (Figure 5c,d), and the embryos were comparable to E5.5 embryos in vivo (S1c,d). The EOMES-positive ExE cavity and the SOX2-positive EPI cavity merged to form the proamniotic cavity on day 4 of in vitro culture (Figure 5e,f). At this stage, the embryos were similar to E6.5 embryos in vivo (S1e,f). On day 5 of in vitro culture, T-positive cells appeared in the posterior region of the embryo and migrated to the anterior region of the embryo on day 7 (Figure 5g and 5i). FOXA2-positive cells appeared in the anterior and middle regions of the embryo on day 6 of in vitro culture. They were mainly concentrated in the anterior region of the embryo on day 7 of in vitro culture (Figure 5h and 5j). At this stage, the embryos were similar to E7.5 embryos in vivo (S1g–j). After the egg cylinder formation, the yolk sac directly contacting the medium rapidly expanded to form a sphere, and the extraembryonic tissue formed by the EOMES-positive cells underwent apoptosis, resulting in the separation of the extraembryonic tissue and the spherical embryo, and the embryo floats in the medium. These results demonstrate that

the anisotropic microporous scaffolds can support embryos for at least 7 days in vitro. The 30° and 60° anisotropic microporous scaffolds had a suitable wettability for embryo growth and moderate porosity, resulting in a smaller spreading area and a higher proportion of OCT4-positive cells, which supported embryonic development (Figure 6).

4 | DISCUSSION

This study investigated the effect of 3D-printed anisotropic microporous scaffolds on the in vitro development of mouse embryos. Compared with 2D PDMS, 3D-printed PDMS anisotropic microporous scaffolds have more advantages for in vitro embryo culture. Embryos on 2D PDMS are more conducive to developing extraembryonic tissues, forming a larger contact area between embryos. Anisotropic microporous scaffolds with printing angles of 0°, 30°,
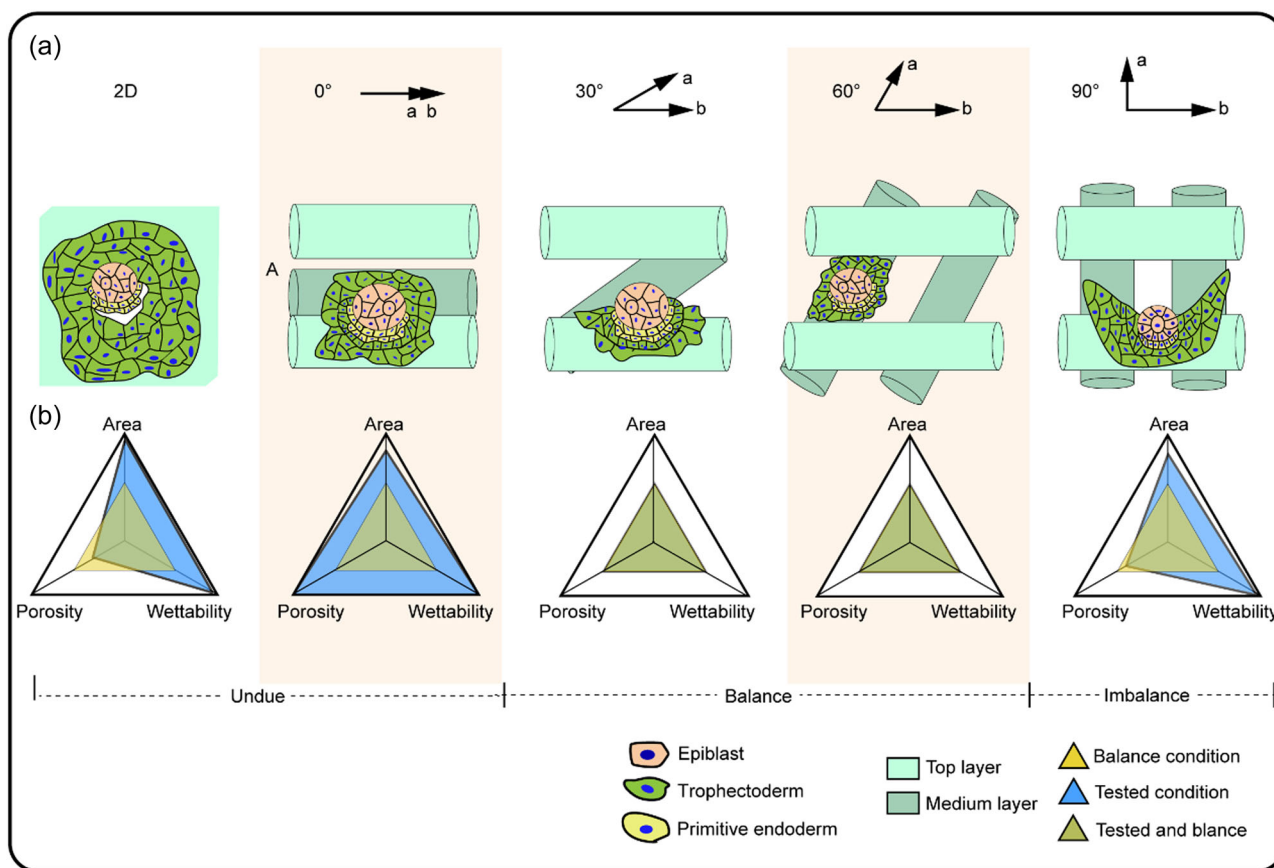

FIGURE 6 Schematic depicting the effect of different angles of PDMS scaffolds and 2D PDMS on the development of embryos. (a) Diagram of in vitro culture day 2 embryo culture on 2D PMDS, 0°, 30°, 60° and 90° PDMS scaffolds. The embryos of 0° microporous stands more prone to contact between the printed fibers, the embryos of 90° anisotropic microporous scaffolds were more prone to contact between or on the fibers. The embryos of 30° and 60° anisotropic microporous scaffolds were more inclined to contact the bevel. (b) Summary of the area of embryo implantation and the porosity of different angle scaffolds. 2D PDMS had a small porosity, large wettability and attachment area. The 0° anisotropic microporous scaffolds had a higher porosity, large wettability, and relatively large attachment area. The 30° anisotropic microporous scaffolds had suitable porosity, wettability, and attachment area. The 60° anisotropic microporous scaffolds had suitable porosity, wettability, and attachment area. The 90° anisotropic microporous scaffolds had large wettability, smaller porosity and relatively large attachment area. PDMS, polydimethylsiloxane.

60°, and 90° could effectively reduce the development of extra-embryonic tissue. The 30° and 60° anisotropic microporous scaffolds could better support embryo development in vitro and extend the in vitro development time of mouse embryos.

PDMS has a wide range of biomedical applications because of its transparent, elastomeric, biocompatible, gas-permeable, water-impermeable, relatively inexpensive and superior printing performance (Bhattacharjee et al., 2018). The modulus of PDMS is comparable to that of the uterus (Kolahi et al., 2012), and PDMS has been tried in embryo culture to study external mechanical forces exerted by the interaction between embryo and maternal uterine tissues (Hiramatsu et al., 2013). It has been reported that a contact angle of 40°–60° is beneficial for cell growth (Lee et al., 1998; Menzies & Land Jones, 2010). And cell spreading is much greater on hydrophilic surfaces (Wei et al., 2007). But long term incubation of biomaterial in a medium usually induces an increase of the wettability (hydrophilicity) in terms of decreasing water contact angle, affecting cell behaviors in particular proliferation and attachment (Amirikia et al., 2017). The contact angle (wettability) may affect the area of embryo extension, which will require more validation in future. The anisotropic microporous scaffolds formed at 0° had a large porosity, causing the embryos to be more prone to contact between the printed fibers. The anisotropic microporous scaffolds formed at 90° had a small porosity, which resulted in the embryos being more prone to contact between or on the fibers. The anisotropic microporous scaffolds formed at 30° and 60° provided embryos with wettability that were more suitable for embryo growth compared to 0° and 90°, resulting in embryos that were more inclined to contact the bevel (Laronda et al., 2017). We reasoned that an extensive contact area resulted in the overgrowth of extraembryonic tissue and partial growth restriction of the embryoid body. It could be the reason for poor embryonic development in the 0° and 90° anisotropic microporous scaffolds and 2D PDMS conditions. The 0°, 90° anisotropic microporous scaffolds and 2D PDMS had a higher proportion of EOMES-positive cells, which indicates that the embryos are more capable of developing extraembryonic tissues in the future (Harrison et al., 2017). The 30° and 60° anisotropic microporous scaffolds had a large proportion of OCT4-positive cells, which indicates that the embryo could develop the embryo body in the future (Harrison et al., 2017; Sozen et al., 2018). Conversely, the 30° and 60° anisotropic microporous scaffolds provided a smaller attachment area, resulting in better embryo development.

These results contribute to understanding how scaffolds affect embryonic development and lay the foundation for future in-depth studies of embryonic mechanics in vivo. This study combines developmental biology and engineering to gain insight into implantation mechanisms and provide a platform to understand developmental biological processes.

AUTHOR CONTRIBUTIONS

Qi Gu and Jia Guo: designed the experiments. **Jia Guo and Yuanyuan Li**: performed the experiments and analyzed the results. **Jia Guo**: wrote the manuscript. **Zili Gao, Jiawei Lyu, Wenli Liu, Yongchao Duan, and Lixun Zhou**: provided assistance in carrying out experiments and discussed results. **Qi Gu**: supervised the work and revised the manuscript.

CONFLICTS OF INTEREST

The authors declare no conflicts of interest.

DATA AVAILABILITY STATEMENT

All data are available upon request.

ORCID

Qi Gu http://orcid.org/0000-0001-9387-9525

REFERENCES

Aguilera-Castrejon, A., Oldak, B., Shani, T., Ghanem, N., Itzkovich, C., Slomovich, S., Tarazi, S., Bayerl, J., Chugaeva, V., Ayyash, M., Ashouokhi, S., Sheban, D., Livnat, N., Lasman, L., Viukov, S., Zerbib, M., Addadi, Y., Rais, Y., Cheng, S., ... Hanna, J. H. (2021). Ex utero mouse embryogenesis from pre-gastrulation to late organogenesis. *Nature*, 593(7857), 119–124. -+ https://doi.org/10.1038/s41586-021-03416-3

Amirikia, M., Shariatzadeh, S., Jorsaraei, S., & Soleimani Mehranjani, M. (2017). Impact of pre-incubation time of silk fibroin scaffolds in culture medium on cell proliferation and attachment. *Tissue and Cell*, 49(6), 657–663. https://doi.org/10.1016/j.tice.2017.09.002

Aplin, J., & Dand Ruane, P. T. (2017). Embryo-epithelium interactions during implantation at a glance. *Journal of Cell Science*, 130(1), 15–22. https://doi.org/10.1242/jcs.175943

Bedzhov, I., Leung, C. Y., Bialecka, M., & Zernicka-Goetz, M. (2014). In vitro culture of mouse blastocysts beyond the implantation stages. *Nature Protocols*, 9(12), 2732–2739. https://doi.org/10.1038/nprot.2014.186

Bedzhov, I., & Zernicka-Goetz, M. (2014). Self-Organizing properties of mouse pluripotent cells initiate morphogenesis upon implantation. *Cell*, 156(5), 1032–1044. https://doi.org/10.1016/j.cell.2014.01.023

Bhattacharjee, N., Parra-Cabrera, C., Kim, Y. T., Kuo, A. P., & Folch, A. (2018). Desktop-stereolithography 3D-printing of a poly (dimethylsiloxane)-based material with Sylgard-184 properties. *Advanced Materials*, 30(22), e1800001. https://doi.org/10.1002/adma.201800001

Campo, H., Cervello, I., & Simon, C. (2017). Bioengineering the uterus: An overview of recent advances and future perspectives in reproductive medicine. *Annals of Biomedical Engineering*, 45(7), 1710–1717. https://doi.org/10.1007/s10439-016-1783-3

Carson, D. D., Tang, J., & Pand Gay, S. (1988). Collagens support embryo attachment and outgrowth in vitro: Effects of the Arg-Gly-Asp sequence. *Developmental Biology*, 127(2), 368–375. https://doi.org/10.1016/0012-1606(88)90323-5

Cui, H., Nowicki, M., Fisher, J. P., & Zhang, L. G. (2017). 3D bioprinting for organ regeneration. *Advanced Healthcare Materials*, 6(1):1601118. https://doi.org/10.1002/adhm.201601118

Do, A. V., Khorsand, B., Geary, S. M., & Salem, A. K. (2015). 3D printing of scaffolds for tissue regeneration applications. *Advanced Healthcare*

Materials, 4(12), 1742–1762. https://doi.org/10.1002/adhm.201500168

Engelmayr GC, Jr., Cheng, M., Bettinger, C. J., Borenstein, J. T., Langer, R., & Freed, L. E. (2008). Accordion-like honeycombs for tissue engineering of cardiac anisotropy. Nature Materials, 7(12), 1003–1010. https://doi.org/10.1038/nmat2316

Ferraz, M.A. M. M., Nagashima, J. B., Venzac, B., Le Gac, S., & Songsasen, N. (2020). 3D printed mold leachates in PDMS microfluidic devices. Scientific Reports, 10(1), 994. https://doi.org/10.1038/s41598-020-57816-y

Filas, B. A., Bayly, P., & Vand Taber, L. A. (2011). Mechanical stress as a regulator of cytoskeletal contractility and nuclear shape in embryonic epithelia. Annals of Biomedical Engineering, 39(1), 443–454. https://doi.org/10.1007/s10439-010-0171-7

Fu, J. P., Warmflash, A., & Lutolf, M. P. (2021). Stem-cell-based embryo models for fundamental research and translation. Nature Materials, 20(2), 132–144. https://doi.org/10.1038/s41563-020-00829-9

Govindasamy, N., Long, H., Jeong, H. W., Raman, R., Özcifci, B., Probst, S., Arnold, S. J., Riehemann, K., Ranga, A., Adams, R. H., Trappmann, B., & Bedzhov, I. (2021). 3D biomimetic platform reveals the first interactions of the embryo and the maternal blood vessels. Developmental Cell, 56(23), 3276–3287. https://doi.org/10.1016/j.devcel.2021.10.014

Gu, Z., Guo, J., Wang, H., Wen, Y., & Gu, Q. (2020). Bioengineered microenvironment to culture early embryos. Cell Proliferation, 53(2), e12754. https://doi.org/10.1111/cpr.12754

Harrison, S. E., Sozen, B., Christodoulou, N., Kyprianou, C., & Zernicka-Goetz, M. (2017). Assembly of embryonic and extraembryonic stem cells to mimic embryogenesis in vitro. Science, 356(6334):eaal1810. https://doi.org/10.1126/science.aal1810

He, X. (2017). Microscale biomaterials with bioinspired complexity of early embryo development and in the ovary for tissue engineering and regenerative medicine. ACS Biomaterials Science & Engineering, 3(11), 2692–2701. https://doi.org/10.1021/acsbiomaterials.6b00540

Hiramatsu R, Matsuoka T, Kimura-Yoshida C, Han S.W., Mochida K., Adachi T., Takayama S., Matsuo I., (2013), External mechanical cues trigger the establishment of the anterior-posterior axis in early mouse embryos. Developmental Cell, 27(2): 131-144. https://doi.org/10.1016/j.devcel.2013.09.026

Hollister, S. J. (2006). Porous scaffold design for tissue engineering. Nature Materials, 5(7), 518–524. https://doi.org/10.1038/nmat1683

Hossain, N., Chowdhury, M. A., Shuvho, M., Kashem, M. A., & Kchaou, M. (2021). 3D-Printed objects for multipurpose applications. Journal of Materials Engineering and Performance, 30(7), 4756–4767. https://doi.org/10.1007/s11665-021-05664-w

Hsu, Y. C. (1973). Differentiation in vitro of mouse embryos to the stage of early somite. Dev Biol, 33(2), 403–411. https://doi.org/10.1016/0012-1606(73)90145-0

Huang, G., Li, F., Zhao, X., Ma, Y., Li, Y., Lin, M., Jin, G., Lu, T. J., Genin, G. M., & Xu, F. (2017). Functional and biomimetic materials for engineering of the three-dimensional cell microenvironment. Chemical Reviews, 117(20), 12764–12850. https://doi.org/10.1021/acs.chemrev.7b00094

Huang, T. Q., Qu, X., Liu, J., & Chen, S. (2014). 3D printing of biomimetic microstructures for cancer cell migration. Biomedical Microdevices, 16(1), 127–132. https://doi.org/10.1007/s10544-013-9812-6

Hull, S. M., Brunel, L., & Gand Heilshorn, S. C. (2022). 3D bioprinting of cell-laden hydrogels for improved biological functionality. Advanced Materials, 34(2), e2103691. https://doi.org/10.1002/adma.202103691

Kauma, S., & Wand Matt, D. W. (1995). Coculture cells that express leukemia inhibitory factor (lif) enhance mouse blastocyst development in-vitro. Journal of Assisted Reproduction and Genetics, 12(2), 153–156. https://doi.org/10.1007/Bf02211386

Kolahi, K. S., Donjacour, A., Liu, X., Lin, W., Simbulan, R. K., Bloise, E., Maltepe, E., & Rinaudo, P. (2012). Effect of substrate stiffness on early mouse embryo development. PLoS One, 7(7), 10. https://doi.org/10.1371/journal.pone.0041717

Laronda, M. M., Rutz, A. L., Xiao, S., Whelan, K. A., Duncan, F. E., Roth, E. W., Woodruff, T. K., & Shah, R. N. (2017). A bioprosthetic ovary created using 3D printed microporous scaffolds restores ovarian function in sterilized mice. Nature Communications, 8, 15261. https://doi.org/10.1038/ncomms15261

Lee, J. H., Khang, G., Lee, J. W., & Lee, H. B. (1998). Interaction of different types of cells on polymer surfaces with wettability gradient. Journal of Colloid and Interface Science, 205(2), 323–330. https://doi.org/10.1006/jcis.1998.5688

Liu, X., Wang, X., Zhang, L., Sun, L., Wang, H., Zhao, H., Zhang, Z., Liu, W., Huang, Y., Ji, S., Zhang, J., Li, K., Song, B., Li, C., Zhang, H., Li, S., Wang, S., Zheng, X., & Gu, Q. (2021). 3D liver tissue model with branched vascular networks by multimaterial bioprinting. Advanced Healthcare Materials, 10(23):e2101405. https://doi.org/10.1002/adhm.202101405

Ma, Z., Koo, S., Finnegan, M. A., Loskill, P., Huebsch, N., Marks, N. C., Conklin, B. R., Grigoropoulos, C. P., & Healy, K. E. (2014). Three-dimensional filamentous human diseased cardiac tissue model. Biomaterials, 35(5), 1367–1377. https://doi.org/10.1016/j.biomaterials.2013.10.052

Manoogian, S. J., Bisplinghoff, J. A., McNally, C., Kemper, A. R., Santago, A. C., & Duma, S. M. (2008). Dynamic tensile properties of human placenta. Journal of Biomechanics, 41(16), 3436–3440. https://doi.org/10.1016/j.jbiomech.2008.09.020

Menzies, K., & Land Jones, L. (2010). The impact of contact angle on the biocompatibility of biomaterials. Optometry and Vision Science, 87(6), 387–399. https://doi.org/10.1097/OPX.0b013e3181da863e

Ozbolat, V., Dey, M., Ayan, B., Povilianskas, A., Demirel, M. C., & Ozbolat, I. T. (2018). 3D printing of PDMS improves its mechanical and cell adhesion properties. ACS Biomaterials Science & Engineering, 4(2), 682–693. https://doi.org/10.1021/acsbiomaterials.7b00646

Peng, K., Liu, X., Zhao, H., Lu, H., Lv, F., Liu, L., Huang, Y., Wang, S., & Gu, Q. (2021). 3D bioprinting of reinforced vessels by dual-cross-linked biocompatible hydrogels. ACS Applied Bio Materials, 4(5), 4549–4556. https://doi.org/10.1021/acsabm.1c00283

Plachta, N., Bollenbach, T., Pease, S., Fraser, S. E., & Pantazis, P. (2011). Oct4 kinetics predict cell lineage patterning in the early mammalian embryo. Nature Cell Biology, 13(2), 117–U124. https://doi.org/10.1038/ncb2154

Raja, N., & Yun, H. S. (2016). A simultaneous 3D printing process for the fabrication of bioceramic and cell-laden hydrogel core/shell scaffolds with potential application in bone tissue regeneration. Journal of Materials Chemistry B: Materials for Biology and Medicine, 4(27), 4707–4716. https://doi.org/10.1039/c6tb00849f

Salomon, D., & Sand Sherman, M. I. (1975). Implantation and invasiveness of mouse blastocysts on uterine monolayers. Experimental Cell Research, 90(2), 261–268. https://doi.org/10.1016/0014-4827(75)90315-8

Shahbazi, M. N., Scialdone, A., Skorupska, N., Weberling, A., Recher, G., Zhu, M., Jedrusik, A., Devito, L. G., Noli, L., Macaulay, I. C., Buecker, C., Khalaf, Y., Ilic, D., Voet, T., Marioni, J. C., & Zernicka-Goetz, M. (2017). Pluripotent state transitions coordinate morphogenesis in mouse and human embryos. Nature, 552(7684), 239–243. -+ https://doi.org/10.1038/nature24675

Sozen, B., Amadei, G., Cox, A., Wang, R., Na, E., Czukiewska, S., Chappell, L., Voet, T., Michel, G., Jing, N., Glover, D. M., & Zernicka-Goetz, M. (2018). Self-assembly of embryonic and two extra-embryonic stem cell types into gastrulating embryo-like structures. Nature Cell Biology, 20(8), 979–989. https://doi.org/10.1038/s41556-018-0187-z

Wang, H., Guo, K., Zhang, L., Zhu, H., Li, S., Li, S., Gao, F., Liu, X., Gu, Q., Liu, L., & Zheng, X. (2021). Valve-based consecutive bioprinting method for multimaterial tissue-like constructs with controllable interfaces. *Biofabrication*, 13(3), 035001. https://doi.org/10.1088/1758-5090/abdb86

Wang J., Wang L., Feng G, Wang Y., Li Y., Li X., Liu C., Jiao G., Huang C., Shi J., Zhou T., Chen Q., Liu Z., Li W., Zhou Q., (2018), Asymmetric expression of LincGET biases cell fate in two-cell mouse embryos. *Cell*, 175(7): 1887-1901. https://doi.org/10.1016/j.cell.2018.11.039

Wei, J., Yoshinari, M., Takemoto, S., Hattori, M., Kawada, E., Liu, B., & Oda, Y. (2007). Adhesion of mouse fibroblasts on hexamethyldisiloxane surfaces with wide range of wettability. *Journal of biomedical materials research. Part B, Applied biomaterials*, 81(1), 66–75. https://doi.org/10.1002/jbm.b.30638

Weimar, C. H., Post Uiterweer, E. D., Teklenburg, G., Heijnen, C. J., & Macklon, N. S. (2013). In-vitro model systems for the study of human embryo-endometrium interactions. *Reproductive BioMedicine Online*, 27(5), 461–476. https://doi.org/10.1016/j.rbmo.2013.08.002

Wu, T. C., Wan, Y., & Jand Damjanov, I. (1981). Positioning of inner cell mass determines the development of mouse blastocysts in vitro. *Journal of Embryology and Experimental Morphology*, 65, 105–117.

Yang, H., Sun, L., Pang, Y., Hu, D., Xu, H., Mao, S., Peng, W., Wang, Y., Xu, Y., Zheng, Y. C., Du, S., Zhao, H., Chi, T., Lu, X., Sang, X., Zhong, S., Wang, X., Zhang, H., Huang, P., ... Mao, Y. (2021). Three-dimensional bioprinted hepatorganoids prolong survival of mice with liver failure. *Gut*, 70(3), 567–574. https://doi.org/10.1136/gutjnl-2019-319960

Yoo, D. (2013). New paradigms in hierarchical porous scaffold design for tissue engineering. *Materials Science and Engineering: C Materials for Biological Applications*, 33(3), 1759–1772. https://doi.org/10.1016/j.msec.2012.12.092

Zegers-Hochschild, F., Adamson, G. D., de Mouzon, J., Ishihara, O., Mansour, R., Nygren, K., Sullivan, E., van der Poel, S., International Committee for Monitoring Assisted Reproductive, T., & World Health, O. (2009). The International Committee for monitoring assisted reproductive technology (ICMART) and the World Health Organization (WHO) revised glossary on ART terminology, 2009. *Human Reproduction*, 24(11), 2683–2687. https://doi.org/10.1093/humrep/dep343

Zheng, H., & Xie, W. (2019). The role of 3D genome organization in development and cell differentiation. *Nature Reviews Molecular Cell Biology*, 20(9), 535–550. https://doi.org/10.1038/s41580-019-0132-4

Zhou, X., Nowicki, M., Sun, H., Hann, S. Y., Cui, H., Esworthy, T., Lee, J. D., Plesniak, M., & Zhang, L. G. (2020). 3D Bioprinting-tunable small-diameter blood vessels with biomimetic biphasic cell layers. *ACS Applied Materials & Interfaces*, 12(41), 45904–45915. https://doi.org/10.1021/acsami.0c14871

Zhu, M., Li, W., Dong, X., Yuan, X., Midgley, A. C., Chang, H., Wang, Y., Wang, H., Wang, K., Ma, P. X., Wang, H., & Kong, D. (2019). In vivo engineered extracellular matrix scaffolds with instructive niches for oriented tissue regeneration. *Nature Communications*, 10(1), 4620. https://doi.org/10.1038/s41467-019-12545-3

SUPPORTING INFORMATION

Additional supporting information can be found online in the Supporting Information section at the end of this article.